Short communication

# Detection of water vapor in cathode gas diffusion layer of polymer electrolyte fuel cell using water sensitive paper

Kosuke Nishida [a,*], Motoyuki Ishii [a], Shohji Tsushima [b], Shuichiro Hirai [b]

[a] Department of Mechanical and System Engineering, Kyoto Institute of Technology, Matsugasaki, Sakyo-ku, Kyoto 606-8585, Japan
[b] Department of Mechanical and Control Engineering, Tokyo Institute of Technology, 2-12-1 Ohokayama, Meguro-ku, Tokyo 152-8552, Japan

A B S T R A C T

Water management in cathode electrode of polymer electrolyte fuel cell (PEFC) is essential for high performance operation, because liquid water condensed in porous gas diffusion layer (GDL) and catalyst layer (CL) blocks oxygen transport to active reaction sites. In this study, the water vapor distribution inside the cathode GDL of a PEFC was detected by using water sensitive paper (WSP) to understand the water transport through the cathode electrode during the startup. Furthermore, the liquid water behavior at the cathode was directly visualized using an optical diagnostic, and the water distribution under the current-collecting ribs and gas channels of the cathode separator was investigated. It was found that the water vapor concentration within the cathode electrode begins to increase near the CL in the downstream region immediately after starting the operation. In the cathode upstream region, the water concentration becomes remarkably high under the current-collecting ribs of the cathode separator because the ribs block the water vapor exhaust from the cathode GDL.

© 2011 Elsevier B.V. All rights reserved.

## 1. Introduction

Polymer electrolyte fuel cell (PEFC) is a promising candidate for mobile and vehicle applications and distributed power systems because of its high power density and low operating temperature. However, there are several technical problems to be solved in order to achieve practicability and popularization. Especially, water management inside the porous gas diffusion layer (GDL) of a PEFC is essential for high performance operation. At a high current density, excessive water generated by the cathode electrode reaction is rapidly condensed in the porous GDL. When the open pores inside the cathode GDL are filled with liquid water, oxygen cannot be sufficiently supplied to the reaction sites. This phenomenon known as "water flooding" is critical barrier for high efficiency and high power density. In order to solve this issue, it is necessary to understand the fundamental phenomenon of the water transport inside the cathode GDL.

In recent years, visualization studies to probe water transport in operating PEFCs have been conducted by many researchers. Liquid water formation, accumulation and removal inside PEFCs were investigated by neutron radiography [1–8], soft X-ray radiography [9], X-ray computed tomography [10,11], and optical visualization using transparent fuel cells [12–16]. Water content distribution in

polymer electrolyte membrane (PEM) was measured by using magnetic resonance imaging (MRI) [17]. Among these methods, neutron radiography has the significant advantage that the structural materials commonly used for fuel cell are transparent to neutrons. Thus, water distribution in fuel cell can be visualized without the use of optical-transparent or non-conducting special materials, and quantitatively evaluated. However, in most conventional experiments of neutron radiography, neutron beam for probing passes perpendicular to PEM surface, which is called "through-plane imaging". This method cannot distinguish between water residing in anode and cathode compartment. Recently, Boillat et al. [8] succeeded in probing a cross section of the membrane electrode assembly (MEA) in a working fuel cell using high-resolution neutron imaging, and resolved the water distribution between the different layers composing the fuel cell for the first time. In this report, the water distribution in the cathode GDL was quantitatively investigated based on so-called "in-plane imaging", it was distinguished under the ribs and channels. In addition, Sasabe et al. [9] applied soft X-ray radiography technique to visualizing the liquid water in an operating fuel cell. The liquid water distribution within the porous GDL and the discharge behavior under the cathode ribs were successfully observed by the high-resolution "in-plane visualization" test. Sinha et al. [11] quantitatively studied the distribution of liquid water saturation inside the GDL of a PEFC using X-ray microtomography. Although many experimental studies for visualizing water distribution in optically opaque fuel cell have been attempted, the efforts to clearly distinguish water distribution inside thin cathode

---

* Corresponding author. Tel.: +81 75 724 7321; fax: +81 75 724 7300.
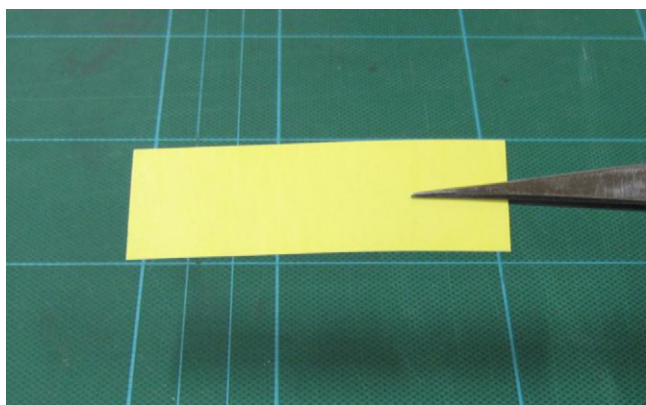E-mail address: knishida@kit.ac.jp (K. Nishida).

**Fig. 1.** Water sensitive paper (WSP).



**Fig. 2.** Discoloration of WSP when exposed to high humidity environments at 20 °C ((a) RH = 80% and (b) RH = 90%).

GDL are few. While optical visualization has been widely employed for visualizing two-phase flow phenomena in transparent cell, the observable region is limited to the flow channels.

On the other hand, modeling studies to understand two-phase flow across cathode GDL and catalyst layer (CL) have been also conducted [18–22]. He et al. [18] and Natarajan and Nguyen [19] proposed two-dimensional two-phase models for cathode of PEFCs with interdigitated and conventional flow fields, respectively. Pasaogullari and Wang [21] developed a theory describing liquid water transport in a hydrophobic GDL and explored the effect of GDL wettability on liquid water transport in detail for the first time. In addition, Das et al. [22] developed a simplified mathematical formulation of liquid water transport in cathode CL and provided the one-dimensional analytical solutions for the hydrophilic and hydrophobic CLs. Recently, Sinha and Wang [23,24], Gostick et al. [25] and Rebai and Prat [26] have developed a pore-network model to understand the liquid water transport in a hydrophobic GDL with the GDL morphology taken into account. Although various two-phase models for a porous GDL, which include capillary transport of liquid water, have been proposed as mentioned above, the experimental validation of these models is not sufficiently discussed.

This paper presents a novel method for measuring the water vapor distribution within the cathode GDL of a PEFC using water sensitive paper (WSP). WSP is a test paper for detecting high humidity, and makes it possible to understand the water vapor transport inside the GDL. Although visualization of high-resolution spatial distribution of liquid water in GDL has been successfully carried out by using neutron radiography [8], soft X-ray radiography [9] and X-ray microtomography [11], these equipments for measurement are special and expensive. The WSP measurement method proposed in this study can only detect high-concentrated water vapor within the cathode GDL on the short-term cell operation. However, from the results of the WSP measurement, we can qualitatively predict the liquid water distribution which would be formed later inside the GDL after long-term operation without the use of specialized equipment. Furthermore, the liquid water behavior at the cathode is directly visualized using an optical diagnostic, and the water transport under the current-collecting ribs and channels of the cathode separator is discussed.

## 2. Experimental

### 2.1. Water sensitive paper (WSP)

To elucidate the water vapor transport inside the cathode GDL of an operating fuel cell, water sensitive paper (WSP), which is a rigid test paper for water detection manufactured by Syngenta, is used in this experiment. Fig. 1 shows the photograph of WSP. The
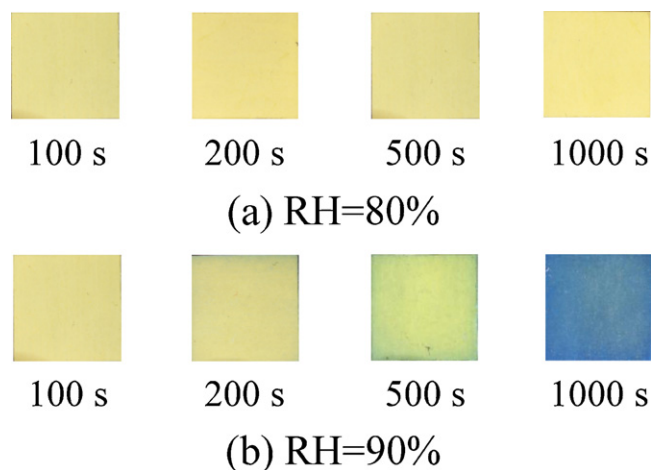
thickness of WSP is approximately 100 μm. WSP is coated with a yellow surface, which is irreversibly changed into dark blue when exposed to high humidity and aqueous spray. The porosity and pore size of WSP are much less than those of GDL, and the gas permeability is extremely lower. In addition, the surface wettability is somewhat hydrophobic, and therefore liquid droplets do not penetrate into WSP. During fuel cell operation, WSP is installed inside the cathode GDL of the assembled cell. The color image of water distribution recorded on the paper is visualized ex-situ by a CCD camera after operation test. Fig. 2 presents the discoloration images of WSP when exposed to two different high humidity environments at 20 °C. When the relative humidity is 80%, the yellow surface is not changed into blue for 1000 s. On the other hand, at the relative humidity of 90%, the WSP surface begins to discolor from yellow to blue at $t$ = 500 s.

### 2.2. Experimental fuel cell

Fig. 3(a) shows the schematic diagram of the fuel cell used in this experiment. The catalyst coated membrane (CCM, PEM: Nafion-115) on which platinum particles (0.5 mg cm$^{-2}$) are loaded is sandwiched between two PTFE-proofed GDLs (Toray TGP-H type carbon paper) without a microporous layer (MPL). In addition, the MEA constructed of the PEM, two CLs and two GDLs is sandwiched between two copper current collector plates with gold coating. The active electrode area is 5.0 cm$^2$. Two stainless steel separators which have a single-pass serpentine flow channel are placed outside the current collectors and held together by four M6 bolts. A sheet of WSP (1.0 mm width and 30 mm length) is installed inside the double-layered GDL on the cathode side, which is composed of two thin carbon papers (TGP-H-030, 060 and 090), as seen in Fig. 3(a). The GDL on the anode side is TGP-H-120 (360 μm thick). In order to directly observe the liquid water behavior at the cathode electrode using a digital CCD camera, a quartz glass is inserted into the cathode separator as a window. Pure hydrogen and oxygen as the fuel and oxidant are fed into the anode and cathode channels without humidification. The utilizations of H$_2$ and O$_2$ are 0.15 and 0.03, respectively. The operating temperature and pressure are 20 °C and 1 atm. In actual PEFC stacks, high temperature (70–80 °C) and high humidity operations are generally selected. However, water flooding can also occur at low temperature operations such as cold startup and outdoor operation. The conditions in this experiment are valid during these operations of fuel cells. Fig. 3(b) presents the schematic of the single-serpentine flow channel in the cathode separator. The width, depth and overall length
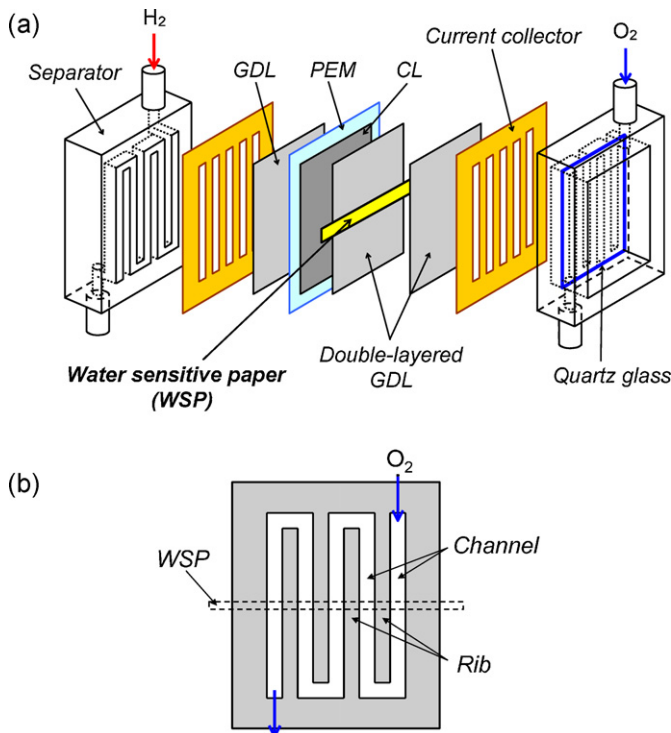
**Fig. 3.** Schematic diagram of the experimental fuel cell ((a) cell structure and (b) serpentine flow field in the cathode separator).



**Fig. 5.** Influence of WSP insertion on the $I$–$V$ characteristic of the experimental fuel cell at 20 °C.

Fig. 4 shows three installation positions of WSP in the cross-section of the cathode GDL. In each figure, C1, C2, C3, C4 and C5 denote five gas channels in the serpentine flow field. R1, R2, R3 and R4 are the current-collecting ribs of the cathode separator. Oxygen gas streams from the right channel (C1) to the left channel (C5) along the serpentine flow field. Position (1) is located at the interface between the cathode GDL and stainless steel separator. In the case of the installation of WSP in Position (1), a WSP sheet is sandwiched between TGP-H-120 (360 mm thick) and the current-collecting plate. Positions (2) and (3) are located 190 and 110 μm away from the CL surface, respectively. When WSP is inserted into these two positions, the double-layered structure, which is composed of two thin carbon papers, is applied to the cathode GDL. In case of the installation in Position (2), WSP is sandwiched between two TGP-H-060 (190 μm thick) carbon papers. In Position (3), WSP is sandwiched between TGP-H-030 (110 μm thick) and TGP-H-090 (280 μm thick). A WSP sheet is inserted in the in-plane direction of the GDL. At the insertion position of WSP, the groove-type pocket to hold a 100 μm thick WSP sheet is formed by electrical discharge machining. Thus, the interfacial contact resistance is not increased by the WSP insertion.

The influence of WSP insertion on the fuel cell performance is discussed in Fig. 5. This figure shows the current–voltage ($I$–$V$) curves for the two cases with and without WSP. These $I$–$V$ measurements were conducted after the pre-operation of the cell. The anode and cathode gases are dry $H_2$ and $O_2$ at 20 °C, respectively. The MEA used in this measurement is composed of a Nafion-115 membrane, CLs and TGP-H-060 GDLs. In the case with WSP, a WSP sheet is inserted into the interface between the cathode GDL and current collector. It is noted that the $I$–$V$ curve for the case with WSP is almost similar to that for the case without WSP. This result indicates the WSP sheet does not increase the contact resistance at the insertion position. Since the gas permeability of WSP is much less than that of GDL, oxygen gas inside the GDL detours around the WSP sheet and arrives late at the reaction sites. In addition, liquid water generated at the catalyst layer is prevented from being discharged from the GDL by the WSP insertion. However, in this study, the operation test for the WSP measurement is carried out under the low-current of 0.1 or 0.2 A cm$^{-2}$ and the short-term of 100–300 s conditions. At a low current density, the consumption of oxygen and the production of water at the cathode CL are extremely little. Therefore, it is expected that the oxygen supply to the reaction sites is sufficient even if the WSP sheet is inserted in the GDL. Furthermore, the amount of liquid water generated in the CL is not much because of the short-term operation. Under these mild conditions, severe water flooding does not occur inside the GDL, and
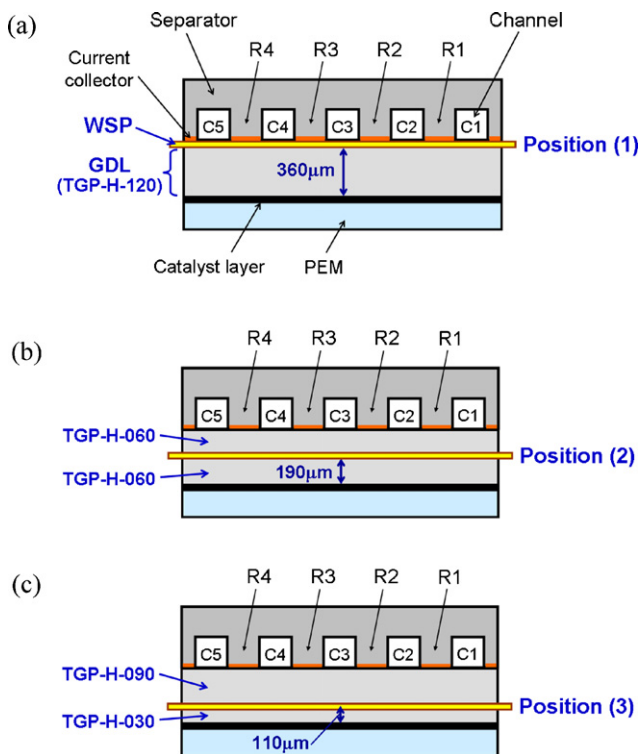


**Fig. 4.** Installation positions of WSP in the cross-section of the cathode GDL ((a) GDL/separator interface, (b) Intermediate region and (c) near catalyst layer).

are 2.0 mm, 2.0 mm and 10.5 cm, respectively. Pure $O_2$ flows from the upper right to the lower left. The WSP sheet is positioned in the center of the cathode flow field, as shown in this figure.
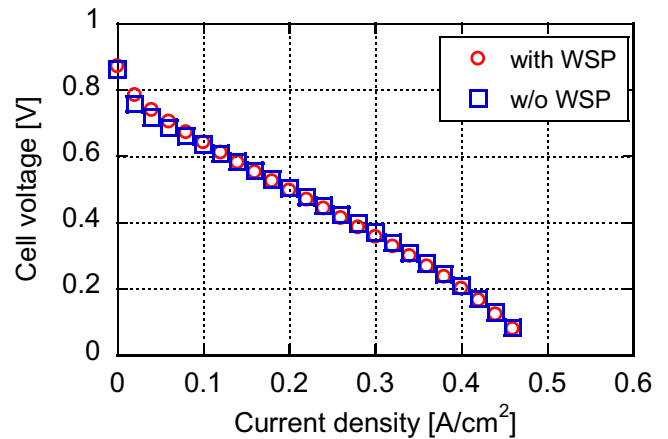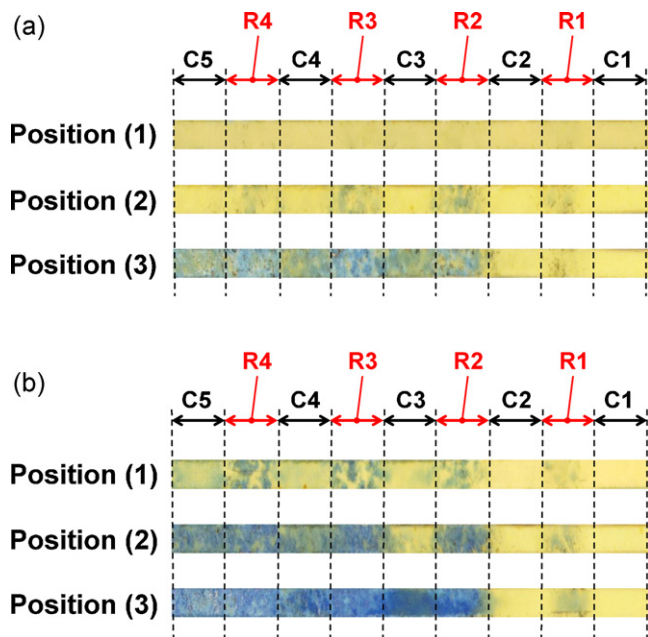
**Fig. 6.** Images of WSP discoloration inside the double-layered cathode GDL after (a) 100 and (b) 200 s of operation at 0.1 A cm$^{-2}$. Positions (1), (2) and (3) are the installation positions of WSP across the GDL thickness shown in Fig. 4.

the damage from the WSP insertion to the fuel cell performance is not significant. Since the WSP sheet is not directly touched to the CL surface, the active reaction area is not reduced at all by the WSP insertion.

### 2.3. Experimental procedure

The experimental procedure in this study is as follows:

(1) The pre-operation of the experimental fuel cell is carried out at 20 °C and 0.16 A cm$^{-2}$ for 30 min to hydrate the electrolyte membrane.
(2) After the pre-operation, the assembled cell is decomposed and the wet MEA is slowly dried until the high frequency resistance (HFR) of the electrolyte membrane is adjusted to 600 mΩ cm$^2$, which is the initial operating condition.
(3) The experimental cell is assembled again, and a WSP sheet is inserted into the double-layered cathode GDL. Subsequently, the constant-current startup test is conducted at 20 °C under non-humidity condition, and the liquid drop behavior is optically observed through the transparent window by using a digital CCD camera.
(4) After the fuel cell operation, the WSP sheet is removed from the assembled cell, and the discoloration image of the WSP is captured ex-situ using the camera.

## 3. Results and discussion

### 3.1. Water vapor distribution inside cathode GDL

Fig. 6 shows the images of the WSP discoloration due to the absorption of high-concentrated water vapor inside the cathode GDL after 100 and 200 s of operation. The current density is set to 0.1 A cm$^{-2}$. Each image was observed ex-situ after the WSP sheet was removed from the assembled cell. Positions (1), (2) and (3) denote the three installation positions of WSP through the GDL thickness shown in Fig. 4. When a WSP sheet is inserted into Positions (2) and (3), the double-layered GDL structure is applied. C1,
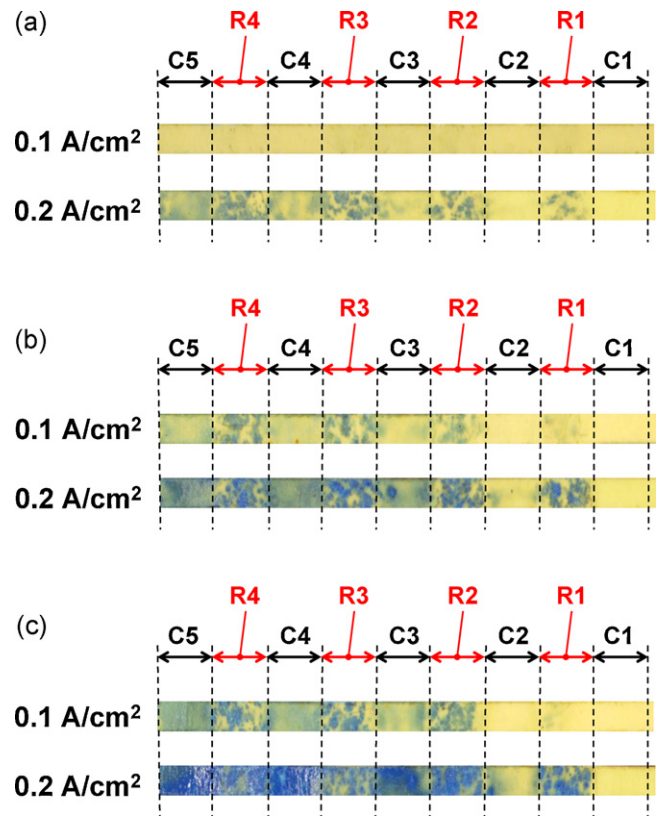


**Fig. 7.** Effect of current density on the WSP discoloration in Position (1) after (a) 100, (b) 200 and (c) 300 s of operation. The current density is set to 0.1 and 0.2 A cm$^{-2}$ as a parameter.

C2, C3, C4 and C5 are located under the flow channels. R1, R2, R3 and R4 are located under the current-collecting ribs. The cathode gas flows from the right channel (C1) to the left channel (C5) along the serpentine flow field. These six images of WSP were obtained from different six operation tests. Furthermore, in each position, several experiments were repeated to confirm the reproducibility of the WSP measurement results. After 100 s of the startup, the WSP sheet begins to discolor into blue gradually from the catalyst layer in the cathode downstream region because of the water generation. Furthermore, as seen in Position (2) at $t$ = 100 s, the water vapor concentration first increases under the ribs of the cathode separator. This indicates that the current-collecting ribs block the water vapor exhaust from the cathode CL and GDL. Consequently, the water vapor concentration under the ribs becomes higher than that under the flow channels. After 200 s of the operation, the WSP discolors remarkably under the ribs within the cathode GDL owing to the water transport limitation. Since dry O$_2$ gas is supplied to the cathode inlet, the WSP hardly discolors under the upstream channels of C1 and C2. On the other hand, in the downstream region, the WSP discoloration arises not only under the ribs but also under the channels, because the water vapor concentration in the cathode channel increases monotonically along the flow direction.

### 3.2. Effect of current density on water vapor transport in cathode GDL

Fig. 7 presents the effect of current density on the discoloration of WSP inside the cathode GDL after 100, 200, and 300 s of startup. The current density is set to 0.1 and 0.2 A cm$^{-2}$ as a parameter. These images were individually obtained from different operation tests. The WSP sheet for water detection is installed at the interface between the GDL and separator (Position (1)). At the current
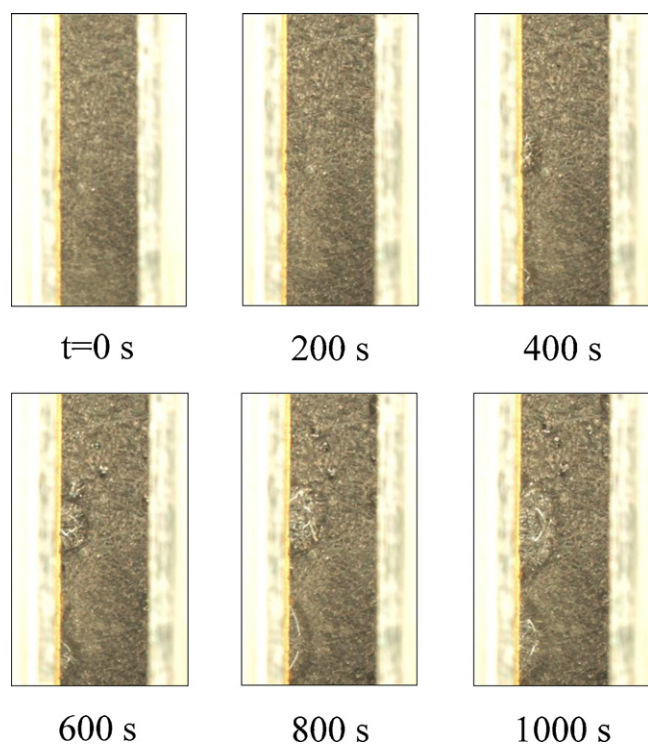
**Fig. 8.** Visualization of liquid water behavior in the upstream channel (C3) during startup at 0.2 A cm$^{-2}$. The photographs were taken after 0, 200, 400, 600, 800 and 1000 s of operation.
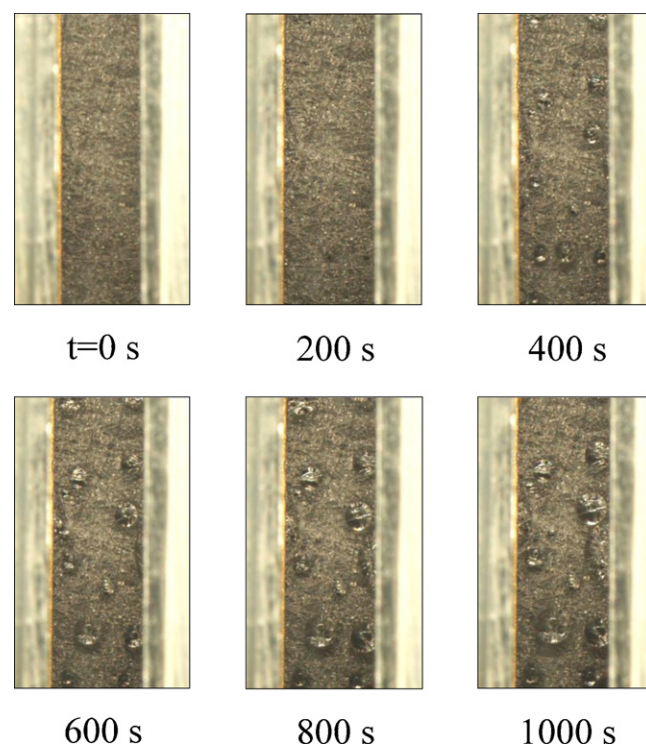


**Fig. 9.** Visualization of liquid water behavior in the downstream channel (C5) during startup at 0.2 A cm$^{-2}$.

density of 0.1 A cm$^{-2}$, the WSP does not discolor after 100 s of operation shown as in Fig. 7(a). On the other hand, when the current density is increased up to 0.2 A cm$^{-2}$, the water vapor concentration within the GDL immediately rises to the saturation level after starting the operation and the WSP is converted into blue under the ribs. In the case of 0.2 A cm$^{-2}$, the WSP discoloration after 200 and 300 s is more remarkable as compared with that in the case of 0.1 A cm$^{-2}$. At $t$ = 300 s, it is expected that more liquid water is generated and accumulated inside the cathode GDL because of high humidity.

### 3.3. Visualization of liquid water behavior at cathode

Figs. 8 and 9 show the sequential images of liquid water behavior in the upstream (C3) and downstream (C5) channels for 1000 s. C3 and C5 denote the third and fifth channels of the serpentine flow field, respectively, as shown in Fig. 4. The current density is set to 0.2 A cm$^{-2}$, and the GDL on the cathode side is TGP-H-120. The liquid droplet behavior inside the channel was optically visualized through the transparent window by using a CCD digital camera. In the upstream channel of C3 shown in Fig. 8, several droplets are discharged from the left corner between the current-collecting rib and GDL, and gradually grown as the time proceeds. This result reveals that much water is condensed mainly under the ribs owing to the transport limitation of water vapor. On the other hand, in the downstream of C5 shown in Fig. 9, many water droplets appear from the GDL surface as well as from the corner between the rib and GDL. This indicates that the liquid water is generated and accumulated not only under the ribs but also under the channels inside the cathode GDL due to the high-humidity gas flow. These characteristics of water condensation agree with the results of the WSP measurement mentioned in Section 3.1.

## 4. Conclusions

To understand the water transport through the cathode GDL of a PEFC, this paper presented a novel method for detecting water vapor distribution inside the GDL using water sensitive paper (WSP). In addition, the liquid water behavior on the cathode side was also visualized by using an optical diagnostic, and the water transport under the current-collecting ribs and gas channels of the separator was discussed. Especially, the following conclusions can be drawn from this study.

(1) The water vapor concentration within the cathode electrode begins to increase gradually from the catalyst layer in the downstream region because of the water generation.
(2) In the cathode upstream, the water vapor concentration inside the GDL first increases under the current-collecting ribs because the ribs block the water vapor exhaust from the CL and GDL. On the other hand, in the downstream region, the WSP discoloration arises not only under the ribs but also under the channels due to the high-humidity gas flow.
(3) With an increase in current density, the water vapor concentration within the cathode GDL immediately rises to the saturation level under the ribs after starting the operation.
(4) In the upstream region of cathode, since water vapor is condensed mainly under the ribs, liquid water within the GDL is discharged from the corner between the current-collecting rib and GDL into the flow channel. On the other hand, in the downstream, many water droplets are exhausted from the GDL surface as well as from the corner between the rib and GDL.

## References

[1] R.J. Bellows, M.Y. Lin, M. Arif, A.K. Thompson, D. Jacobson, J. Electrochem. Soc. 146 (1999) 1099–1103.
[2] R. Satija, D.L. Jacobson, M. Arif, S.A. Werner, J. Power Sources 129 (2004) 238–245.

[3] D. Kramer, J. Zhang, R. Shimoi, E. Lehmann, A. Wokaun, K. Shinohara, G.G. Scherer, Electrochem. Acta 50 (2005) 2603–2614.

[4] J. Zhang, D. Kramer, R. Shimoi, Y. Ono, E. Lehmann, A. Wokaun, K. Shinohara, G.G. Scherer, Electrochem. Acta 51 (2006) 2715–2727.

[5] A. Turhan, K. Heller, J.S. Brenizer, M.M. Mench, J. Power Sources 160 (2006) 1195–1203.

[6] M.A. Hickner, N.P. Siegel, K.S. Chen, D.N. McBrayer, D.S. Hussey, D.L. Jacobson, M. Arif, J. Electrochem. Soc. 153 (2006) A902–A908.

[7] K. Yoshizawa, K. Ikezoe, Y. Tasaki, D. Kramer, E.H. Lehmann, G.G. Scherer, J. Electrochem. Soc. 155 (2008) B223–B227.

[8] P. Boillat, D. Kramer, B.C. Seyfang, G. Frei, E. Lehmann, G.G. Scherer, A. Wokaun, Y. Ichikawa, Y. Tasaki, K. Shinohara, Electrochem. Comm. 10 (2008) 546–550.

[9] T. Sasabe, S. Tsushima, S. Hirai, Int. J. Hydrogen Energy 35 (2010) 11119–11128.

[10] S.J. Lee, N.Y. Lim, S. Kim, G.G. Park, C.S. Kim, J. Power Sources 185 (2008) 867–870.

[11] P.K. Sinha, P. Halleck, C.Y. Wang, Electrochem. Solid-State Lett. 9 (2006) A344–A348.

[12] K. Tüber, D. Pócza, C. Hebling, J. Power Sources 124 (2003) 403–414.

[13] X.G. Yang, F.Y. Zhang, A.L. Lubawy, C.Y. Wang, Electrochem. Solid-State Lett. 7 (2004) A408–A411.

[14] F.Y. Zhang, X.G. Yang, C.Y. Wang, J. Electrochem. Soc. 153 (2006) A225–A232.

[15] K. Nishida, T. Murakami, S. Tsushima, S. Hirai, J. Power Sources 195 (2010) 3365–3373.

[16] S. Litster, D. Sinton, N. Djilali, J. Power Sources 154 (2006) 95–105.

[17] S. Tsushima, K. Teranishi, S. Hirai, Electrochem. Solid-State Lett. 7 (2004) A269–A272.

[18] W. He, J.S. Yi, T.V. Nguyen, AIChE J. 46 (2000) 2053–2064.

[19] D. Natarajan, T.V. Nguyen, J. Electrochem. Soc. 148 (2001) A1324–A1335.

[20] Z.H. Wang, C.Y. Wang, K.S. Chen, J. Power Sources 94 (2001) 40–50.

[21] U. Pasaogullari, C.Y. Wang, J. Electrochem. Soc. 151 (2004) A399–A406.

[22] P.K. Das, X. Li, Z.S. Liu, Int. J. Hydrogen Energy 35 (2010) 2403–2416.

[23] P.K. Sinha, C.Y. Wang, Electrochem. Acta 52 (2007) 7936–7945.

[24] P.K. Sinha, C.Y. Wang, Chem. Eng. Sci. 63 (2008) 1081–1091.

[25] J.T. Gostick, M.A. Ioannidis, M.W. Fowler, M.D. Pritzker, J. Power Sources 173 (2007) 277–290.

[26] M. Rebai, M. Prat, J. Power Sources 192 (2009) 534–543.